



Highly sensitive V-shaped SPR PCF biosensor for cancer detection

M. Abdelghaffar^{1,3,4} · Yusuf Gamal^{2,4} · Reda A. El-Khoribi¹ · Wafaa Soliman³ · Y. Badr³ · Mohamed Farhat O. Hameed^{4,5,6} · S. S. A. Obayya^{4,7}

Received: 16 January 2023 / Accepted: 2 March 2023 / Published online: 3 April 2023
© The Author(s) 2023

Abstract

In this paper, a novel design of photonic crystal fiber (PCF) biosensor based on surface plasmon resonance (SPR) is introduced and analyzed for cancer cell detection. The full vectorial finite element method (FVFEM) is used throughout the numerical analysis of the suggested biosensor. The reported PCF has a V-shaped surface that is coated with ZrN as a plasmonic material. A coupling occurs between the core guided mode and surface plasmon mode SPM which depends on the studied analyte. Such a coupling is improved by using the suggested V-shape geometry which increases the sensor sensitivity. The geometrical parameters are optimized to achieve high sensor sensitivity. The proposed biosensor has high optical sensitivity of 6214.28, 3800, and 5008.33 nm/RIU, for quasi-transverse magnetic (TM), and 6000 nm/RIU, 4400 nm/RIU, and 5333.3 nm/RIU, for quasi-transverse magnetic (TE), for breast, basal, and cervical cancer cells, respectively. The reported optical sensor can pave the way for efficient and simple technique for cancer detection with low cost and high sensitivity instead of surgical and chemical techniques.

Keywords Biomedical sensor · Photonic crystal fiber · Cancer cell detection · Surface plasmon resonance

1 Introduction

Photonic crystal fiber (PCF) (Hameed et al. 2011) is a distinctive and special class of optical fibers that has attracted a lot of attention due to its advantages with wide range of applications. PCFs have high birefringence (Sharma et al. 2013), (Hameed et al. 2009a, b) large mode area (Raja and Varshney 2014), infinitely single mode operation (Akowuah et al. 2009), tunable dispersion (Hsu et al. 2015), and low loss (Bradley et al. 2013). Therefore, PCFs have been used for different applications such as polarization handling devices (Hameed and Obayya 2010) (Younis et al. 2018), and

✉ Mohamed Farhat O. Hameed
mfarahat@zewailcity.edu.eg

✉ S. S. A. Obayya
sobayya@zewailcity.edu.eg

couplers (Hameed, Obayya and Wiltshire 2009a, b). Additionally, PCFs serve as a sensor platform for magnetic field (Nallusamy et al. 2017), low refractive index (RI) (Gamal et al. 2022a, b), vibration (Zhao et al. 2014), strain (Villatoro et al. 2007), and temperature (Gamal et al. 2022a, b). Moreover, PCF-based chemical and biological sensors have been designed for the detection of glucose (Luo et al. 2014), pH (W. Li et al. 2013), salinity (Vigneswaran et al. 2018), cholesterol (Soylemez et al. 2015), DNA (Sun et al. 2014) and early cancer detection (Abdelghaffar et al. 2022).

Surface plasmon resonance (SPR) at metal/dielectric interface can be used for sensing, imaging, scanning, and other fields. The sensing mechanism depends on the interaction between the guided core modes and the SPM. The resonance occurs at the phase matching wavelength where the effective indices of the SPM and core mode are identical. Then maximum power transfers occur from the core guided mode to the SPM at the resonance wavelength at which depends on the dielectric optical properties, plasmonic PCFs have been used in many applications, such as (RI) sensors (Maier and Atwater 2005), temperature sensors (Gamal et al. 2022a, b), gas sensors (Rifat et al., 2019), and pressure sensors (Osório et al. 2014). In this context, D-shaped configuration is a good choice for SPR-PCF sensor. Luan et al., have reported a plasmonic D-shaped PCF RI sensor with sensitivity of 2900 nm/RIU (Luan et al. 2015). Additionally, D-shaped PCF-SPR with ITO and graphene coating layers has been designed with sensitivity of 5700 nm/RIU (Patnaik et al. 2015). Further, D-shaped PCF-SPR (Wang et al. 2016) has been introduced based on internal gold coating through the core region with a sensitivity of 6430 nm/RIU. Recently, Yusuf et al. have investigated a dual D-shaped plasmonic PCF RI sensor with sensitivity of 11,000 nm/RIU. In order to increase the light confinement in the studied analyte at the metal/dielectric interface, several modifications for the D-shaped PCF sensors have been reported ((Liu et al. 2019), and (Wójcik et al. 2010). Highly birefringent PCF fiber has been also suggested for sensing the hydrostatic pressure (Wójcik et al. 2010). Further, (Liu et al. 2019) have designed micro-structure optical fiber sensor with sensitivities of 3376 nm/RIU and 2.65 nm/°C for RI and temperature measurement, respectively. Additionally, SPR-PCF sensor based on silver internally coated layer experimentally published with sensitivity of 1800 nm/RIU (Klantsataya et al. 2015). Further, SPR-PCF has been experimentally fabricated using polymer side hole coated with gold for fluid sensing with sensitivity of 2000 nm/RIU (Wang et al. 2009). Moreover, D-shaped PCF coated by gold layer has been experimentally fabricated with sensitivity of 3500 nm/RIU (Yu et al. 2011). In addition, externally coated plasmonic PCF biosensor was experimentally demonstrated to measure the binding kinetics of the IgG (anti-IgG) complexes with sensitivity of 2154 nm/RIU (Wong et al. 2013). Further, D-shaped PCF has been designed, fabricated and analyzed for glucose detection with sensitivity of 294.11 nm/RIU (Azab et al., 2022).

Cancer disease is a significant threat for human health therefore; cancer early detection techniques are highly needed. Therefore, plasmonic fiber optic biosensor has been proposed [89] for early detection of breast cancer. Moreover, nano cavity of plasmonic biosensor [88] with sensitivity of 300 nm/RIU has been introduced. In addition, planar SP multimode optical fiber has been demonstrated for RI sensing with sensitivity of 608.6 nm/RIU [91]. Further, dual core PCF with sensitivity 5714.28 for breast cancer cell has been reported. Additionally, breast cancer detection sensor based on PCF (Ramanujam et al. 2019) with sensitivity of 43 nm/RIU has been introduced. Furthermore, a multi-analyte sensing capability has been developed using plasmonic biosensor with four concentric analyte channels [93]. The reported silver/gold doped PCF sensor is characterized with sensitivity of 2500 nm/RIU and 3083 nm/RIU for channel 1 and channel 2, respectively [93].

Jindal et al. have introduced linked photonic crystal (PhC) waveguide cancer detector with sensitivity up to 391 nm/RIU (Jindal et al. 2016).

Conventional plasmonic PCF sensors depend on utilizing silver, gold or bimetallic configuration of gold and silver (Akowuah et al. 2012). The conventional plasmonic materials (Gold and silver) have disadvantages of boarder resonance curves and bad chemical stability, respectively. Thus, new plasmonic materials such as ZrN, TiN, ITO and ZnO are used. The ZrN is refractory plasmonic material with a very high melting point, mechanically strong, abrasion resistant and high chemical stability at temperatures above 2000 °C with CMOS compatibility (El-Saeed et al. 2019). However, ZrN is superior with higher hardness value, less growth rate and texture orientation at higher pulse voltage. (Heinrich et al. 2008), low cost (Monfared, Kurylyk and Dasog, 2022), and best corrosion resistance (Zhang et al. 2022). As a result, ZrN is utilized as a plasmonic material for the proposed device. Further, the reported sensor is externally coated design, which makes it label free, easy to use, more safe, and easy to fabricate.

In recent years, *gold/TiO₂* coated PCF biosensor was presented for breast cancer cells which offers sensitivities of 11,034 nm/RIU and 9,285 nm/RIU for x- and y-polarized core modes, respectively, with resolution in the range of 10^{-6} RIU (Verma, Kumar and Jindal, 2022). Further, photonic crystal (DPhC) was suggested for cancerous brain tumors detection, using *SiO₂* nanoparticles embedded in a superconducting material layer. The reported biosensor achieves sensitivity of 4139.24 nm/RIU (Malek et al. 2022). Additionally, SPR PCF biosensor with gold (Au) and titanium dioxide (*TiO₂*) coated layers was proposed for different cancer cell detection with sensitivities of 9428.57 nm/RIU, 10,714.28 nm/RIU, 7571.43 nm/RIU, 5500 nm/RIU, and 6000 nm/RIU for the MDAMB-231, MCF-7, PC12, HeLa, and Jurkat cancerous cells, respectively (Chaudhary, Kumar and Kumar, 2022). Moreover, 1-D binary PhC with a defect layer using (*Si/SiO₂* N/Defect/(*Si/SiO₂*)N structure was introduced for cancer cells detection with sensitivity of 2400.08 nm/RIU (Almawgani et al. 2022). In addition, RI based sensor for skin cancer (Basal, HeLa, MDA-MB-231) detection using silicon rods in the air bed was presented with sensitivity of 3080 nm/RIU (Sani et al. 2022). Additionally, SPR-PCF biosensor for two breast cancer cells detection was developed with sensitivities of 4500 nm/RIU and 4643 nm/RIU for MDA-MB-231 and MCF-7 cancer cells, respectively (Yasli 2022). Moreover, two dimensional random PCF biosensor for breast cancer cells was proposed with sensitivity of 1372.549 nm/RIU (Nayak 2023). Furthermore, 1D PhC based sensor was reported with achieved sensitivity of 73 nm/RIU for cancer cells (Bijalwan et al. 2021). In addition, plasmonic PCF biosensor for cancer detection of a single living cell was developed with sensitivities of 7142.86 nm/RIU and -757 RIU^{-1} for MCF-7, and Hela cell, respectively (Yasli 2021). Plasmonic PCF breast cancer cells biosensor based on ITO coated layer was introduced with sensitivities of 6701.03 nm/RIU and 5154.63 nm/RIU for x- and y-polarization, respectively (Rajeswari and Revathi 2022). Additionally, bottom side polished PCF based biosensor for early cancer detection was presented with sensitivity of 22,857 nm/RIU for blood cancer, 20000 nm/RIU for cervical cancer, 20714 nm/RI for adrenal gland cancer, 20000 nm/RIU for skin cancer, and 21,428, 25,000 nm/RIU for breast cancer (type-1 and type-2)), respectively (Singh and Prajapati 2023).

In this paper, V-shaped SPR PCF sensor is suggested for cancer early detection. The V-groove shape improves the interaction between the core guided mode and SPR mode at the metal/dielectric interface. This helps detect minute variations in the analytes' refractive indices. (Omri et al. 2020). The reported PCF depends on ZrN as a plasmonic material. It's worth noting that, the optimum ZrN thickness layer at the proposed PCF sensor is equal to 40 nm, which makes the device's cost low with respect to others in literature (Kaur and

Singh 2020). Furthermore, dimensions of the sensor are sufficiently large, which makes the fabrication process easier. The geometrical parameters are studied within the allowed fabrication constrains to achieve high sensor sensitivity using full vectorial finite-element method (FVFEM) is used (Obayya et al. 2002). High sensitivities of 6214.28 nm/RIU, 3800 nm/RIU, and 5008.33 nm/RIU, are achieved with resolutions of 2.728×10^{-5} RIU, 2.63×10^{-5} RIU, and 1.92×10^{-5} RIU, for breast, basal and cervical cancer cells, respectively using quasi TM mode. For the quasi TE mode, the suggested design offers corresponding sensitivities of 6000 nm/RIU, 4400 nm/RIU, and 5333.3 nm/RIU, and resolutions of 1.666×10^{-5} RIU, 2.27×10^{-5} RIU, and 1.875×10^{-5} . Further, the analyte is housed in an external channel to facilitate the fabrication process. Additionally, the suggested design could be also used to detect the change in RI for different bio-analyte. Moreover, the achieved sensitivity is greater than that has been reported in (Jabin et al. 2019), (Ayyanar et al. 2018), (Ramanujam et al. 2019), (Jindal et al. 2016), (Sani et al. 2022), (Almawgani et al. 2022), (Malek et al. 2022), (Yasli 2022), (Nayak 2023), and (Ramanujam et al. 2019).

2 Design considerations

Figure 1 shows the 2D cross section of the suggested PCF biosensor. A background of silica is used where air holes of radius $r=2.35 \mu\text{m}$ are arranged in a hexagonal lattice with a hole pitch $\Lambda=6.73 \mu\text{m}$. Further, the upper surface is etched at a distance $h=8.5 \mu\text{m}$ from the PCF center. The V-groove is then made with a distance $x=13.6 \mu\text{m}$ between the two vertices of the V-shape. The etched surface is coated by ZrN layer with a thickness $t=30 \text{ nm}$. The studied analyte covers the plasmonic layer as shown in Fig. 1a. In the same context, Fig. 1(b) shows the sensing system where the laser source is coupled to the PCF biosensor through single mode fiber (SMF) (Luo et al. 2019). Further, SMF will also connect the transmitted light to the spectrometer in order to detect the transmission and hence the losses through the suggested device. High-resolution optical spectrum analyzer (OSA) can be used to show the measured data (Koshiba and Saitoh, 2003). The coupling between the core mode and SPM depends on the analyte RI. At a given RI, a maximum peak of confinement loss is obtained. The analyte RI fluctuation can be detected by measuring the shift in the resonance wavelength.

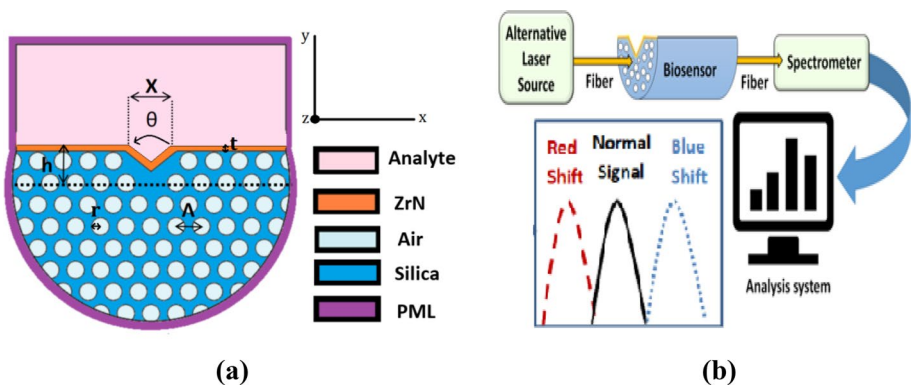


Fig. 1 **a** 2D cross-section of the suggested SPR PCF sensor, and **b** the optical sensing system

The initial geometrical parameters of the suggested design are illustrated in Table 1. The RI of the silica background material is calculated from the following Sellmeier equation (Gamal et al. 2021a, b):

$$n_s^2(\lambda) = 1 + \frac{B_1\lambda^2}{\lambda^2 - C_1} + \frac{B_2\lambda^2}{\lambda^2 - C_2} + \frac{B_3\lambda^2}{\lambda^2 - C_3} \quad (1)$$

where n_s is the RI of the silica, and λ is the wavelength in μm . B_1 , B_2 and B_3 are equal to 0.69616630, 0.40794260, and 0.89747940, respectively. Also C_1 , C_2 and C_3 are given by 0.004679148260, 0.01351206310, and 97.93400250 μm^2 , respectively.

The permittivity of the ZrN is calculated by the following Drude model (Naik et al. 2013).

$$\epsilon_{\text{ZrN}}(\omega) = \epsilon_b - \frac{\omega_p^2}{\omega(\omega + i\gamma_p)} + \frac{f_1\omega_1^2}{(\omega_1^2 - \omega^2 + i\omega\gamma_1)} \quad (2)$$

such that $\epsilon_b = 3.4656$, $\omega_p = 8.018$ eV, $\gamma_p = 0.5192$ eV, $f_1 = 2.4509$, $\omega_1 = 5.48$ eV, and $\gamma_1 = 1.7369$ eV. The confinement loss of the studied modes is calculated from the imaginary part of the mode effective index (El-Saeed et al. 2019).

$$\text{Loss} = \frac{40\pi}{\ln(10)\lambda} \times \text{Im}(n_{\text{eff}}) \times 10^4 \approx 8.686 \times \text{Im}(n_{\text{eff}}) \times 10^4 \frac{\text{dB}}{\text{cm}} \quad (3)$$

where $\text{Im}(n_{\text{eff}})$ is the imaginary part of the complex effective index of the core guided modes. Moreover, the sensor sensitivity $S_\lambda(\lambda)$ can be calculated as (Gamal et al. 2021a, b):

$$S_\lambda(\lambda) = \frac{\partial \lambda_{\text{peak}}}{\partial n_{\text{analyte}}} \quad (4)$$

where λ_{peak} is the resonance wavelength with maximum losses, and n_{analyte} is the analyte RI.

The proposed biosensor can be fabricated using one of several well-known processes (Gupta and Sharma, 2006), including, the sol-gel casting approach (Bise and Trevor, 2005), and drilling (Liu et al. 2010, 2019). Furthermore, the fused array fabrication approach can be utilized to implement air holes with a radius of 0.1 μm or greater in a uniform shape (Falkenstein and Justus, 2013). Through strict process control, the placement of the air holes in the cladding zone could be precisely regulated. In addition, the PCF can be polished in a D-shaped pattern, as reported in (Wang et al. 2009). The D-shaped PCF can be then transformed into a V-shaped cross section as follows. First, a thin silica coating

Table 1 THE initial parameters of the suggested V shape ZRN PCF biosensors

Parameter	Description	Initial values in μm
Λ	Hole pitch of the air holes	6.73
r	Radius of the air hole	2.35
t	Thickness of the ZrN layer	0.30
h	Polishing depth	8.5
x	Distance between V-shape vertices	13.6

is applied to the surface of the D-etched surfaces. Electron-beam lithography can be used to create a slit pattern. Then, HF solution etching will be used to remove the silica film in the slit area. After that, the PCF will be immersed in a 25 percent tetramethylammonium hydroxide (TMAH) solution to etch the V-shaped groove into the silica layer. The initial incision width in the silica mask and the etching duration can be used to control the depth of the V-groove (Migita et al., 2014). Further, the V-groove can be obtained by using wheel polishing technique (Luo et al. 2021) which is more straightforward, and precise. Finally, a high-pressure chemical vapor deposition technique can be used to coat the ZrN layer over the V-shaped PCF structure (Hassani and Skorobogatiy, 2006). Furthermore, analyte penetration on the PCF's outer surface can be accomplished easily by pumping the analyte over the plasmonic material (Kaur and Singh 2020).

3 Numerical results and discussion

The suggested design is studied and analyzed using COMSOL Multiphysics software package 5.4 (<https://www.comsol.com/>) via 2D, radio frequency, electromagnetic waves, frequency domain (emw) model. In this study, computational domain of ($74\mu\text{m} \times 74\mu\text{m}$) is used with outer PCF radius of $37\mu\text{m}$. The computational domain is discretized with total number of elements of 51,956, minimum element size of $0,0223\mu\text{m}$, maximum element size of $4.97\mu\text{m}$ and 1,086,496 degrees of freedom. Perfectly matched layer (PML) (Koshiba and Tsuji, 2000) is applied to the transverse directions to truncate the simulation domain. Further, extensive convergence tests are performed to ensure the numerical accuracy and stability of the results for the proposed sensor. The convergence occurs when the PML thickness is $\geq 1.7\mu\text{m}$ at wavelength $\lambda = 600\text{ nm}$. Therefore, a PML with a thickness of $2.0\mu\text{m}$ is applied with a scale factor 1. The proposed design is utilized to detect the RI variation of the studied analyte with different types of cancer cells such as; breast, cervical and basal cells. The RI range for such cancer types varies from 1.3919 to 1.4009 while the normal cell varies from 1.35 to 1.37 as shown in Table 2.

Figure 2 shows the dispersion of the effective RI of the core mode and SPM and the loss spectrum of the core mode at normal breast cell with $n_a = 1.385$. It may be seen that maximum loss takes place at a resonance wavelength of 612 nm where maximum power transfer occurs from the core mode to the SP mode. It is also evident from the inset field plot that the core mode has more leakage at the resonance wavelength toward the metal/dielectric interface with more power loss. In this case, the effective indices of the core mode and SPM are equal. In order to achieve high spectral sensitivity, the geometrical parameters of

Table 2 RI for basal, breast, and cervical cancer and their normal cells

Cell name	Concentration	RI
Basal cell	Cancer (80%)	1.38(Yaroslavsky et al. 2012)(Tsai and Huang 2012)
	Normal (40–60%)	1.36(Yaroslavsky et al. 2012)(Tsai and Huang 2012)
Breast cell(MDA-MD 231)	Cancer (80%)	1.399(Tsai and Huang 2012) (Sharan et al. 2014)
	Normal (40–60%)	1.385(Tsai and Huang 2012) (Sharan et al. 2014)
Cervical Cell (HeLa)	Cancer (80%)	1.392((Tsai and Huang 2012) (Sharan et al. 2014)
	Normal (40–60%)	1.368(Tsai and Huang 2012) (Sharan et al. 2014)

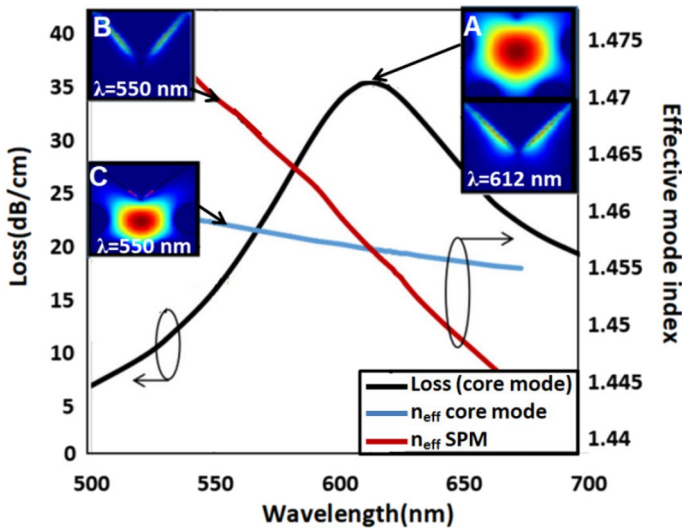


Fig. 2 Variation of wavelength dependent (n_{eff}) of the core mode and SP mode, and losses of the core mode for normal cell with RI of 1.385. The inset figure presents the field plots of a core mode at phase matching point at $\lambda=612$ nm, and **b** (SPM) and **c** core mode at $\lambda=550$ nm, respectively

the biosensor are optimized in the allowed range for the fabrication process, as summarized in Table 3.

Figure 3 depicts a comparison between the D-shaped PCF and the suggested V-shape design at $r=2.35$ μm , $\Lambda=6.73$ μm , and $t=30$ nm where the RI of the analyte changes from $n_a=1.385$ to $n_a=1.399$. Figure 3 shows the loss peak and field plots of the quasi TM mode of the V and D shaped PCFs, at $\lambda=550$ nm and 800 nm respectively. It may be seen that a good coupling is achieved using the V-shape design for both analyte refractive indices. On the other hand, the resonance wavelength of the D-shape structure at $n_a=1.399$ is not strong with broad absorption spectrum. Therefore, V-shaped PCF is suggested with a good coupling between the core mode and SP mode.

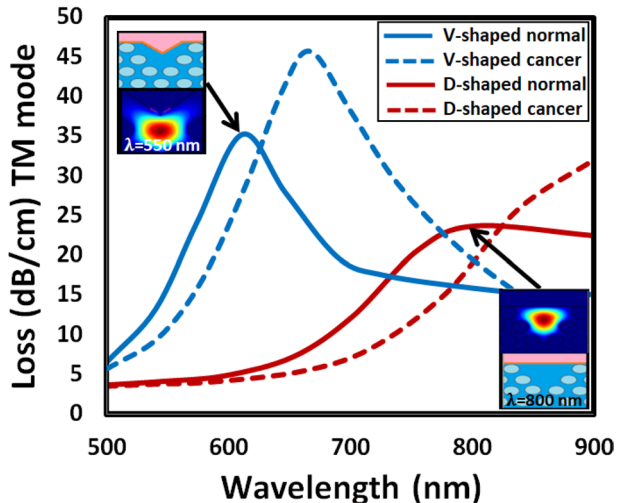
In order to increase the sensor sensitivity for breast cancer detection, the geometrical parameters are studied. The effect of the cladding air holes radius (r) is first investigated and depicted in Fig. 4. However, the other parameters are fixed at their initial values, where $\Lambda=6.73$ μm , $x=13.6$ μm , and $t=30$ nm. The studied r values are 2.3 μm , 2.35 μm , and 2.4 μm , while the analyte RI changes from $n_a=1.385$ to $n_a=1.399$ for breast cancer cell. It is evident from Fig. 4a, b and Table 3 that the air hole radius has a slight effect on the resonance wavelength of the two polarized modes at different analyte refractive indices. This is due to the well confinement of the two polarized modes in the core region. The resulted resonance wavelength peaks of the quasi TM are slightly red shifted and sensitivity is slightly increased from 4000 nm/RIU to 4071 nm/RIU, while the resonance peak and resonance peak shift are fixed for the quasi TE mode. On the other side, the variation of r has no impact on the SPM's effective index. According to Fig. 4 and Table 3, high sensor sensitivity achieves its maximum value at $r=2.35$ μm , which is used in the next study.

The effect of the pitch size Λ is also investigated. Figures 5a, b show the loss spectra of the quasi TM and quasi TE modes, respectively, while the other parameters are equal to $r=2.35$ μm , $x=13.6$ μm , and $t=30$ nm. For quasi TM core mode, with increasing Λ from 6.6 μm , 6.73 μm , the resonance peak at $n_a=1.399$ is slightly red shifted

Table 3 Optimized parameters, resonance wavelength, and corresponding sensitivities of quasi TE and TM modes for breast cancer cell detection

Parameter	$\lambda_{TMpeak}(\mu m)$		$\lambda_{TEpeak}(\mu m)$		Quasi TM sensitivity (nm/RIU)	Quasi TE sensitivity (nm/RIU)
	Normal	Cancer	Normal	Cancer		
$r(\mu m)$						
2.3	0.613	0.668	0.611	0.666	3928.6	3928.6
2.35	0.612	0.669	0.611	0.666	4071	3928.6
2.4	0.612	0.668	0.610	0.664	4000	3857.14
Pitch size (μm)						
6.6	0.613	0.668	0.611	0.666	3928.6	3928.6
6.73	0.612	0.669	0.611	0.666	4071.4	3928.6
6.8	0.612	0.667	0.611	0.666	3928.6	3928.6
$t(nm)$						
20	0.518	0.545	0.516	0.544	1928.6	2000
30	0.612	0.669	0.611	0.666	4071.4	3928.6
40	0.688	0.765	0.686	0.761	5500	5357.14
$x(\mu m)$						
12.4	0.688	0.765	0.686	0.760	5500	5285.7
13.6	0.698	0.777	0.694	0.769	5500	5357.14
15.2	0.706	0.786	0.704	0.782	5714.28	5571.4
16.6	0.714	0.797	0.708	0.789	5928.57	5785.7
18	0.722	0.809	0.718	0.802	6214.28	6000

Fig. 3 Confinement loss spectra of the quasi TM mode for the V-shaped and D-shaped PCF structure at $r=2.35 \mu m$, $\Lambda=6.73 \mu m$, and $t=30 nm$ when the analyte refractive index changes from 1.385 to 1.399. The inset figure shows the field plot of the quasi TM mode of the studied designs at wavelength of 550 nm for V-shaped and 800 nm for D-shaped



from $\lambda = 0.668 \mu m$ to $\lambda = 0.669 \mu m$, and the sensitivity increase from 3928.6 nm/RIU to 4071.4 nm/RIU. This is due to the well confinement of the light in the core region. Therefore, the resonance wave length is slightly affected by the hole pitch variation as shown in

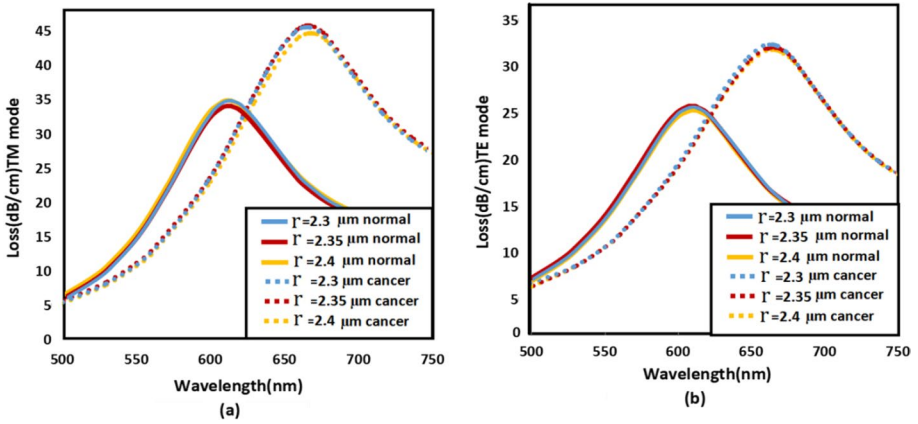


Fig. 4 Confinement loss spectra of **a** the quasi TM and **b** quasi TE modes for different values of r when RI of the analyte changes from 1.385 to 1.399

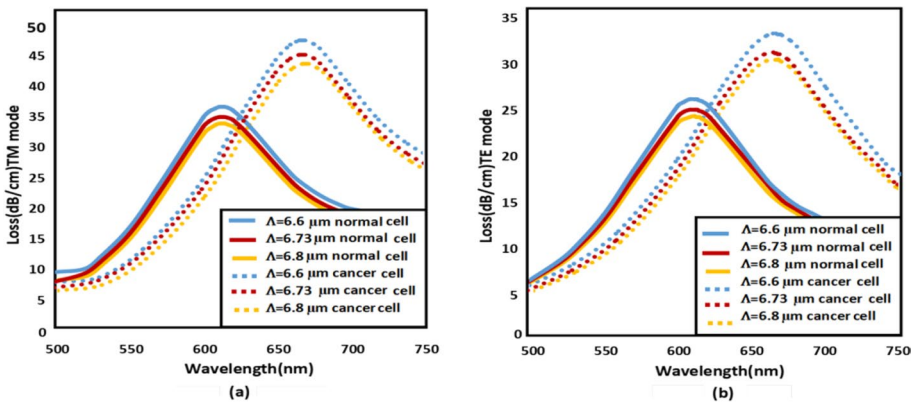


Fig. 5 Confinement loss spectra of **a** the quasi TM and **b** quasi TE modes for different values of Λ when RI of the analyte changes from 1.385 to 1.399

Fig. 5 and Table 3. It may be seen that high sensitivity is obtained at a hole pitch size (Λ) of $6.73 \mu\text{m}$, which is taken in the subsequent studies.

Since the plasmonic material is responsible for SPM excitation owing to the coupling between the core and SPM. Therefore, the effect of the ZrN layer thickness (t) is investigated. Figures 6a, b show the confinement loss of the quasi TM and quasi TE modes at different thickness values of ZrN layer (20, 30, and 40) nm at $n_n = 1.385$ and $n_d = 1.399$. However, the geometrical parameters are fixed at $r = 2.35 \mu\text{m}$, $x = 13.6 \mu\text{m}$, and $\Lambda = 6.73 \mu\text{m}$. It is worth noting from Table 3 and Figs. 6a, b that the loss peak has a red shift from $\lambda = 0.545 \mu\text{m}$ to $\lambda = 0.765 \mu\text{m}$ by increasing the thickness t from 20 to 40 nm. It should be noted that the thickness of the plasmonic material will influence the decay rate of the evanescent wave and SPM. However, the crystallites of ZrN show growth elongation in all directions with increasing deposition temperature. As the thickness is increased by more than 40 nm, the difficulty in the fabrication process will be increased (Sandu et al. 2008).

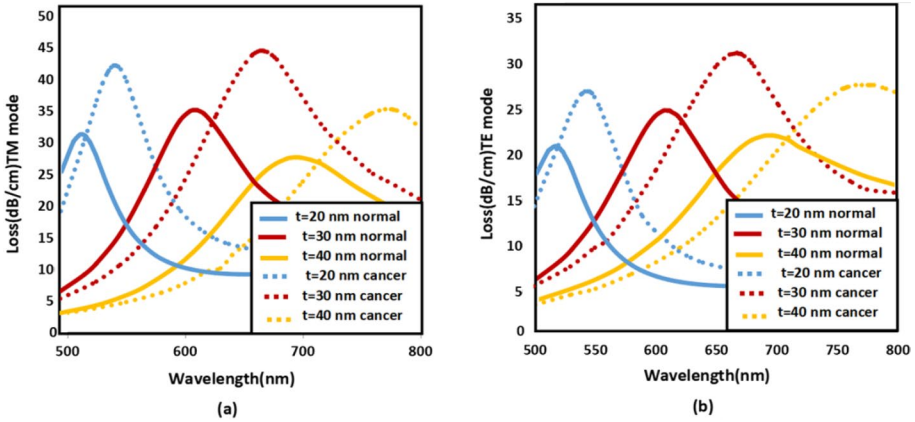


Fig. 6 Confinement loss spectra of **a** the quasi TM and **b** quasi TE modes for different values of thickness t of ZrN, when the RI of the analyte changes from 1.385 to 1.399

Furthermore, the more increasing ZrN thickness, the weaker plasmonic effect, and the more wide confinement loss curve is obtained (Magdi and Swillam 2017). In this curve, the sharpness is reduced as depicted in Figs. 6a, b. At $t=40$ nm, the sensitivity gets its maximum value of 5500 nm/RIU and 5357.14 nm/RIU for the quasi TM and TE modes, respectively. Thus, t is fixed at 40 nm to sustain the maximum sensitivity value.

The impact of the distance x (distance between the two V-shape vertices) is then studied. It is worth mentioning that x reflects the value of angle (θ) at constant depth (h) of the V-groove geometry. Figure 7 depicts the confinement loss spectra of the quasi TM and quasi TE core modes for different values of x (12.4 μm , 13.6 μm , 15.2 μm , 16.6 μm and 18 μm) while the other parameters are taken as $r=2.35$ μm , $\Lambda=6.73$ μm , and $t=40$ nm. It is worth noting from Fig. 7 (a) and (b) that as the analyte RI changes from $n_a=1.385$ for normal cell to $n_a=1.399$ for cancerous cell, the resonance wavelength peaks of the quasi TM and quasi TE modes are red shifted. As the distance x increases, the mode confinement through the core region will also increase. Therefore, the energy transferred to

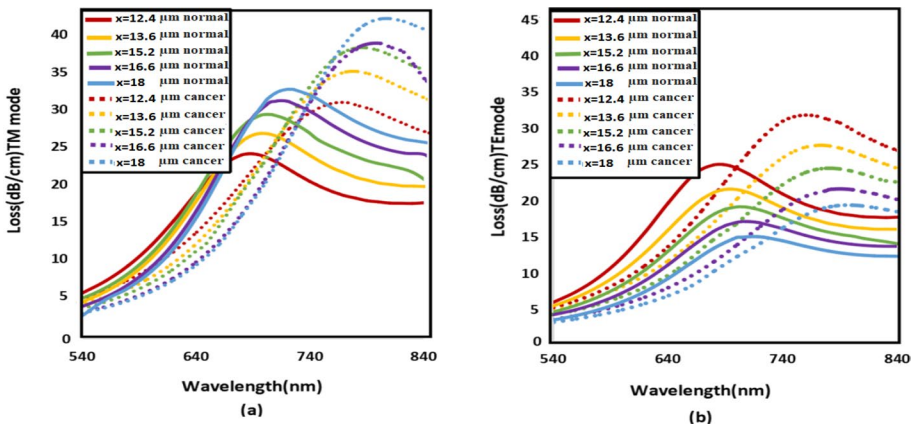


Fig. 7 Confinement loss spectra of **a** the quasi TM and **b** quasi TE modes for different values of X , when the RI of the analyte changes from 1.385 to 1.399

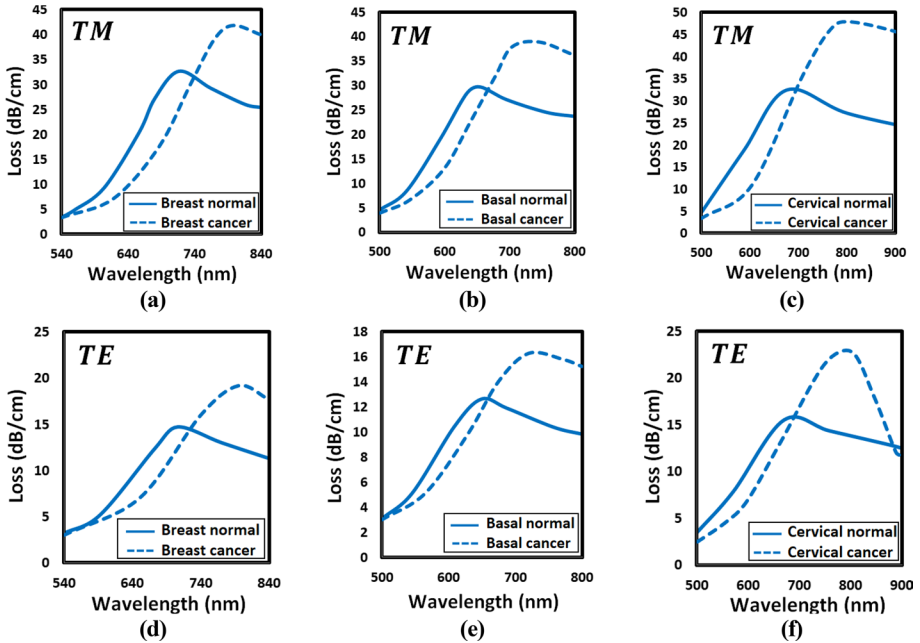


Fig. 8 Confinement loss spectra of the quasi TE and quasi TM mods at normal and cancerous cells of **a, d** breast cell, **b, e** basal cell and **c, f** cervical cell

Table 4 Sensor sensitivities and resolution for breast, basal and cervical cancerous cells

Cancer cell type	TM mode		TE mode	
	Sensitivity nm/RIU	Resolution (RIU)	Sensitivity nm/RIU	Resolution (RIU)
Breast cancer	6214.28	2.728×10^{-5}	6000	1.666×10^{-5}
Basal cancer	3800	2.63×10^{-5}	4400	2.27×10^{-5}
Cervical cancer	5008.33	1.92×10^{-5}	5333.3	1.875×10^{-5}

plasmonic material will be increased with improved sensitivity. The maximum sensitivities of 6214.28 nm/RIU and 6000 nm/RIU for the quasi TM and quasi TE core modes, respectively, is achieved at $x = 18 \mu\text{m}$ ($\theta = 117^\circ$) which is taken as an optimum value. Due to the intersection between the V-groove sides and the nearby air holes, x value cannot be increased more than $18 \mu\text{m}$ which is considered a fabrication limit.

Next, the sensor sensitivity for cancer early detection of other types of cells is studied. Figure 8 shows the confinement loss spectra of the two polarized modes using normal cells, and corresponding cancerous cells including breast, basal and cervical cells. It may be seen from Fig. 8 that the proposed biosensor can detect breast, basal, and cervical cancer cells with sensitivities of 6214.28 nm/RIU, 3800 nm/RIU, and 5008.33 nm/RIU, and good resolution of 2.728×10^{-5} RIU, 2.63×10^{-5} RIU, and 1.92×10^{-5} RIU, respectively, for the quasi TM core mode. Moreover, the suggested design offers sensitivities of 6000 nm/RIU, 4400 nm/RIU, and 5333.3 nm/RIU, and resolution of 1.666×10^{-5} RIU, 2.27×10^{-5} RIU, and 1.875×10^{-5} , respectively, for quasi the TE mode as shown in Table 4.

The linear performance of the proposed design is also investigated. Figure 9a shows the resonance wavelength variation with the analyte RI for quasi TM mode. It is evident that linear fitting can be represented by $\lambda = 4.4 \times 10^3 n - 5.4 \times 10^3$ with coefficient of determination (R^2) and correlation coefficient (r) of 0.9 and 0.95, respectively. Moreover, Fig. 9b depicts the resonance wavelength variation with the RI of the analyte for quasi TE mode where the linear fitting can be represented by $\lambda = 4.3 \times 10^3 n - 5.2 \times 10^3$ with R^2 and r of 0.93 and 0.96, respectively. One of most important parameters for the sensors' quality is the linear relation between the measured value (RI) and its corresponding resonance wavelength. More linearity of the sensor behavior, gives the sensor more accurate measurement along that linear range. The proposed sensor has a good linear response with stable performance. Moreover, it is accurate to predict the resonance wavelength at any given value of refractive index along the RI range from 1.35–1.41.

The resolution of the sensing process is an important metric that can be used to analyze the smallest RI changes. As given by (Gamal et al. 2021a, b).

$$R = \Delta n_a \frac{\Delta \lambda_{\min}}{\Delta \lambda_r} \text{ (RIU)} \tag{5}$$

where $\Delta \lambda_{\min}$ is the wavelength resolution, $\Delta \lambda_r$ is the resonance wavelength shift, and Δn_a is the analyte RI change. In this work, Δn_a is equal to 0.014, $\Delta \lambda_r$ is 81 and 84 nm for quasi TM, and quasi TE mode, respectively, when the analyte RI changes from 1.385 to 1.399. Assuming $\Delta \lambda_{\min}$ is 0.1 nm (Wang et al. 2020), high resolution of the reported bio-sensor will be 2.728×10^{-5} RIU, and 1.666×10^{-5} RIU for quasi TM and TE core modes, respectively.

3.1 Fabrication tolerance study

The fabrication tolerance of the suggested V-shaped PCF sensor is also studied to ensure the robustness of the suggested design to fabrication imperfection. In this study, fabrication tolerance of $\pm 5\%$ is tested (Chang et al., 2019). It is worth mentioning that, only one parameter is studied while the other parameters are fixed at their optimum values. Table 5

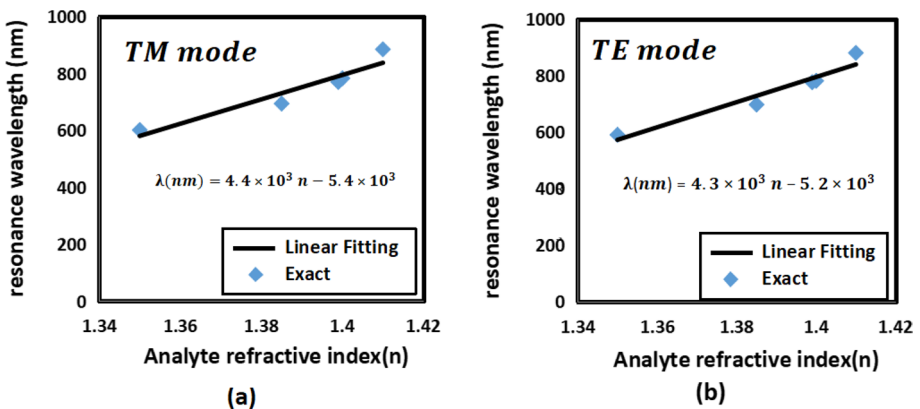


Fig. 9 Linear relation between the RI of the analyte and resonance wavelength for quasi TM and quasi TE mode respectively

Table 5 Fabrication tolerance study of the proposed sensor for the thickness of zrn layer (t), radius of the air holes(r), and distance between the two V-shape vertices (x)

The parameter	Sensitivity nm/RIU / nm/RIU					
	Optimized		$S_{+5\%}$		$S_{-5\%}$	
	TM	TE	TM	TE	TM	TE
t (μm)	6214.28	6000	6614.28	7000	7314.28	7500
r (μm)	6214.28	6000	6214.28	6000	6314.28	6300
x (μm)	6214.28	6000	6199.98	6100	6014.28	6200

shows the tolerance analysis of the thickness of the ZrN layer (t), radius of the air holes (r), and distance between the two V-shape vertices (x) of the proposed design. It is evident that the studied parameters have a good tolerance of $\pm 5\%$ where the sensitivity is still better than 5800 nm/RIU. Therefore, the proposed sensor is feasible for fabrication with good fabrication tolerance.

A comparison between the proposed V-shaped cancer detection sensor with the previously reported sensors in (Sani et al. 2022), (Verma, Kumar and Jindal, 2022), (Chaudhary, Kumar and Kumar, 2022), (Rajeswari and Revathi 2022), (Yasli 2021), (Jabin et al. 2019), (Ayyanar et al. 2018), (Mollah et al. 2020), (Ramanujam et al. 2019), (Jindal et al. 2016), (Abdelghaffar et al. 2022) and (Ramanujam et al. 2019), (Singh and Prajapati 2023), (Almawgani et al. 2022), (Malek et al. 2022), (Yasli 2022), (Nayak 2023) is depicted in Table 6. It is evident that the sensitivity of the proposed early cancer detection biosensor is greater than the introduced biosensors in (Jabin et al. 2019), (Ayyanar et al. 2018), (Ramanujam et al. 2019), (Jindal et al. 2016), (Sani et al. 2022), (Almawgani et al. 2022), (Malek et al. 2022), (Yasli 2022) (Nayak 2023) (Abdelghaffar et al. 2022) and (Ramanujam et al. 2019). Further, the highly sensitive sensors reported in (Verma, Kumar and Jindal, 2022), (Yasli 2021), and (Singh and Prajapati 2023) have used different air hole diameters with complex fabrication process. Further, (Verma, Kumar and Jindal, 2022) and (Singh and Prajapati 2023) have used dual plasmonic materials with higher fabrication cost. In Addition, (Mollah et al. 2020) and (Rajeswari and Revathi 2022) have used internal coating for the plasmonic material through the PCF which is a challenge for fabrication. Further, analyte infiltration will be difficult through the PCF air holes as reported in (Mollah et al. 2020). Moreover, the plasmonic PCF biosensors reported in (Jabin et al. 2019), (Ayyanar et al. 2018), (Mollah et al. 2020), (Ramanujam et al. 2019), (Jindal et al. 2016), (Abdelghaffar et al. 2022) and (Ramanujam et al. 2019) were used to sense either breast or blood cells only, while the suggested biosensor offers early cancer detection for breast, basal and cervical cells.

Surface plasmon sensors have high sensitivity compared to traditional optical biosensing techniques (Azab, Hameed and Obayya, 2023). In addition, surface plasmons based techniques don't need an expert to run the test. However, most of traditional optical sensing techniques can diagnose the cancer at late stages, while surface plasmons can detect cancer in early stages (Azab, Hameed and Obayya, 2023). A comparison between surface plasmons and the colorimetric method and the optical coherence tomography as traditional techniques is introduced in Table 7. It is worth noting from this table that the colorimetric method is the lowest in cost with an average cost of USD~800, while it requires an expert for operation, and high error degrees may arise (González-González et al., 2021). Further, the optical coherence tomography suffers from the highest cost around USD~7164 (Chopra, Wagner and Keane, 2021). On the other hand, surface plasmons have an average cost of USD~6000 (Azab, Hameed and Obayya, 2023).

Table 6 Sensitivity of the proposed V-shaped SPR-PCF biosensor compared to other biosensors in the literature

Ref	Sensor structure	Sensitivity (nm/RIU)
(Wang et al. 2009)	SPR-PCF based on polymer side hole coated with gold	2000
(Yu et al. 2011)	D shaped SPR PCF gold coated sensor	3500
(Wong et al. 2013)	Externally coated plasmonic PCF biosensor	Binding kinetics of the IgG (anti-IgG) complexes with sensitivity of 2154
(Klantsataya et al. 2015)	SPR-PCF sensor based on silver internally coated layer	1800 (RI detection)
(Jindal et al. 2016)	Nanocavity linked PhC waveguide	Up to 391 (RI detection)
(Azzam et al. 2016)	Multichannel PCF biosensor	3083 (RI detection)
(Ayyanar et al. 2018)	Dual core PCF sensor	5714.28 (breast cells)
(Ramanujam et al. 2019)	Photonic crystal (PhC) waveguide sensor	43 (breast cancer)
(Shekar et al. 2019)	Nano cavity plasmonic biosensor	300 (Melanoma cells)
(Walter et al. 2020)	Planner SP multimode sensor	608.6 (RI detection)
(Mollah et al. 2020)	Twin-core PCF sensor	8571.43 (blood cancer detection)
(Bijalwan et al. 2021)	ID PhC based sensor	73 (cancer cells) and 72 (hemoglobin in blood plasma)
(Yasli 2021)	Plasmonic PCF HeLa cancer detection biosensor	7142.86 for MCF-7, and $-757 RIU^{-1}$ for HeLa cell(cancer cells)
(Yasli 2022)	SPR-PCF biosensor, using bending property of PCF	4500 and 4643 for (MDA-MB-231 and MCF-7) breast cancer cells detection
(Abdelghaffar et al. 2022)	V-shaped PCF biosensor	5600 (breast cells)
(Verma, Kumar and Jindal, 2022)	(TiO_2)coated photonic crystal fiber (PCF) biosensor	11,034 in x-polarization, 9,285 in y-polarization (breast cancer cells)
(Malek et al. 2022)	suggested defective photonic crystal (DPhC), using (SiO_2) nanoparticles coat	4139.24 (cancerous brain tumors detection)
(Chaudhary, Kumar and Kumar, 2022)	SPR PCF biosensor using gold (Au) and titanium dioxide (TiO_2) coat	9428.57 (MDAMB-231), 10,714.28 (MCF-7), 7571.43 (PC12), 5500, (HeLa), and 6000 for (Jurkat) cancerous cells
(Almawgani et al. 2022)	ID binary PhC with a defect layer using ($Si/(SiO_2)N$)/Defect/($Si/(SiO_2)N$) structure	2400.08 (cancer cells detection)
(Sani et al. 2022)	refractive index based sensor for using silicon rods in the air bed	between 1294 and 3080 (skin cancer, Basal, HeLa, MDA-MB-231 detection)

Table 6 (continued)

Ref	Sensor structure	Sensitivity (nm/RIU)
(Rajeswari and Revathi 2022)	SPR-PCF biosensor, using ITO layer	6701.03 for x-polarization and 5154.63 for y-polarization.(cancer detection)
(Azab et al., 2022)	Experimental characterization of D-shape PCF RI sensor	294.11 (glucose concentration)
(Nayak 2023)	2D random PhC biosensors	1372.549 (breast cancer cells sensing)
(Singh and Prajapati 2023)	Single core bowl shaped bottom side polished SPR-PCF biosensor	22,857 (blood cancer), 20,000 (cervical cancer), 20,714 (adrenal gland cancer), 20,000 (skin cancer), and 21,428, 25,000 (breast cancer (type-1 and type-2)), respectively
Suggested biosensor	V-shaped SPR-PCF biosensor	6214.28 for Breast Cancer 4400 (basal cells) 5333 (cervical cells)

Table 7 Comparison between surface plasmons and traditional optical techniques

Sensor type	Cost	Cancer detection	Running the test
Colorimetric method (González-González et al., 2021)	USD ~ 800	Detect cancer in late stages	Need expert
Optical coherence tomography (Chopra, Wagner and Keane, 2021)	USD ~ 7164	Detect cancer in late stages	Need expert
Surface plasmons based techniques (Azab, Hameed and Obayya, 2023)	USD ~ 6000	Detect cancer in early stages	Don't need expert

4 Conclusion

A novel V-shaped highly sensitive label-free PCF biosensor based on alternative plasmonic materials is introduced and studied, using FVFEM. The suggested design can be used for breast, basal, cervical cancer detection with sensitivities of 6214.28 nm/RIU, 3800 nm/RIU, and 5008.33 nm/RIU, and resolution of 2.728×10^{-5} RIU, 2.63×10^{-5} RIU, and 1.92×10^{-5} RIU, respectively, for the quasi TM core mode. Further, it offers sensitivities of 6000 nm/RIU, 4400 nm/RIU, and 5333.3 nm/RIU, and resolution of 1.666×10^{-5} RIU, 2.27×10^{-5} RIU, and 1.875×10^{-5} , respectively, for quasi the TE mode. Furthermore, the proposed design has high linearity for the quasi TM and quasi TE modes. The biosensor could be easily fabricated by current PCF fabrication technologies with high fabrication tolerance. Overall, the suggested design is qualified for biological and chemical analyte RI sensing with high sensitivity.

Author contributions MFOH has proposed the idea. MA and YG have done the simulations of the reported sensor. All authors have contributed in the analysis, discussion, writing and revision of the paper. MFOH and SSAO have supervised the work done through the submitted manuscript.

Funding Open access funding provided by The Science, Technology & Innovation Funding Authority (STDF) in cooperation with The Egyptian Knowledge Bank (EKB). The authors acknowledge the financial support from the Science, Technology & Innovation Funding Authority (STIFA) in Egypt under the project (ID: 45702).

Data availability The data will be available upon request.

Declarations

Conflict of interest The authors would like to clarify that there is no financial/non-financial interests that are directly or indirectly related to the work submitted for publication.

Ethical approval The authors declare that there are no conflicts of interest related to this article.

Open Access This article is licensed under a Creative Commons Attribution 4.0 International License, which permits use, sharing, adaptation, distribution and reproduction in any medium or format, as long as you give appropriate credit to the original author(s) and the source, provide a link to the Creative Commons licence, and indicate if changes were made. The images or other third party material in this article are included in the article's Creative Commons licence, unless indicated otherwise in a credit line to the material. If material is not included in the article's Creative Commons licence and your intended use is not permitted by statutory regulation or exceeds the permitted use, you will need to obtain permission directly from the copyright holder. To view a copy of this licence, visit <http://creativecommons.org/licenses/by/4.0/>.

References

- Abdelghaffar, M. *et al.*: Early cancer detection by plasmonic PCF Sensor', 2022 International conference on numerical simulation of optoelectronic devices (NUSOD). IEEE, 147–148 (2022)
- Akowuah, E.K., *et al.*: An endlessly single-mode photonic crystal fiber with low chromatic dispersion, and bend and rotational insensitivity. *J. Lightw. Technol.* IEEE **27**(17), 3940–3947 (2009)
- Akowuah, E.K., *et al.*: Numerical analysis of a photonic crystal fiber for biosensing applications. *IEEE J. Quantum Electron.* IEEE **48**(11), 1403–1410 (2012)
- Almawgani, A.H.M., *et al.*: Highly sensitive nano-biosensor based on a binary photonic crystal for cancer cell detection. *Opt Quantum Electron.* Springer **54**(9), 554 (2022)
- Ayyanar, N., *et al.*: Photonic crystal fiber-based refractive index sensor for early detection of cancer. *IEEE Sens. J.* IEEE **18**(17), 7093–7099 (2018)
- Azab, M. Y., Hameed, M.F.O., Mahdiraji, G.A., Adikan, F.R.M. and Obayya, S.S.A.: Experimental and numerical characterization of a D-shaped PCF refractive index sensor. *Opt. Quantum Electron.* **54**(12), 846 (2022)
- Azab, M.Y., Hameed, M.F.O. and Obayya, S.S.A.: Overview of Optical Biosensors for Early Cancer Detection: Fundamentals, Applications and Future Perspectives. *Biol. (Basel)*. **12**(2), 232 (2023)
- Azzam, S.I., *et al.*: Multichannel photonic crystal fiber surface plasmon resonance based sensor. *Opt Quantum Electron.* Springer **48**(2), 142 (2016)
- Bijalwan, A., Singh, B.K., Rastogi, V.: Analysis of one-dimensional photonic crystal based sensor for detection of blood plasma and cancer cells. *Optik.* Elsevier **226**, 165994 (2021)
- Bise, R.T. and Trevor, D.J.: Sol-gel derived microstructured fiber: fabrication and characterization. In *Optical Fiber Communication Conference*, pp OWL6 (2005)
- Bradley, T.D., *et al.*: Optical properties of low loss (70dB/km) hypocycloid-core kagome hollow core photonic crystal fiber for Rb and Cs based optical applications. *J. Lightw. Technol.* IEEE **31**(16), 3052–3055 (2013)
- Chang, M., Li, B., Chen, N., Lu, X., Zhang, X. and Xu, J.: A compact and broadband photonic crystal fiber polarization filter based on a plasmonic resonant thin gold film. *IEEE Photonics. J.* **11**(2), 1–12 (2019)
- Chaudhary, V. S., Kumar, D. and Kumar, S.: Au-TiO₂ coated photonic crystal fiber based SPR refractometric sensor for detection of cancerous cells. *IEEE Transactions on NanoBioscience.* IEEE. (2022)
- Chopra, R., Wagner, S.K. and Keane, P.A.: Optical coherence tomography in the 2020s—outside the eye clinic. *Eye.* **35**(1), 236–243 (2021)
- El-Saeed, A.H., *et al.*: Highly sensitive SPR PCF biosensors based on Ag/TiN and Ag/ZrN configurations. *Opt. Quantum Electron.* Springer **51**(2), 56 (2019)
- Falkenstein, P. and Justus, B.L.: Fused array preform fabrication of holey optical fibers. *Google Pat.* (2013)
- Gamal, Y., Younis, B.M., Hegazy, S.F., *et al.*: Highly efficient modified dual D-shaped PCF polarization filter. *Opt. Fiber Technol.* Elsevier **62**, 102459 (2021a)
- Gamal, Y., Younis, B. M., Hegazy, Salem F, *et al.*: Highly Sensitive Plasmonic PCF Biosensor. In: 2021b International Applied Computational Electromagnetics Society Symposium (ACES). IEEE, pp. 1–2. (2021b)
- Gamal, Y., Younis, B. M., Hegazy, S. F., *et al.*: Highly sensitive multi-functional plasmonic biosensor based on dual core photonic crystal fiber. *IEEE Sens. J.* IEEE (2022a)
- Gamal, Y., Younis, B. M., Hameed, M. F. O., *et al.*: Plasmonic dual d-shaped PCF sensor for low refractive index applications. In: 2022b International conference on numerical simulation of optoelectronic devices (NUSOD). IEEE, pp. 193–194 (2022b)
- González-González, E., *et al.*: Colloidal loop-mediated isothermal amplification (LAMP) for cost-effective and quantitative detection of SARS-CoV-2: the change in color in LAMP-based assays quantitatively correlates with viral copy number. *Anal. Methods.* **13**(2), 169–178 (2021)
- Gupta, A. and Sharma, A.: Globalization and postcolonial states. *Curr. Anthropol* **47**(2), 277–307 (2006)
- Hameed, M.F.O., Obayya, S.S.A.: Analysis of polarization rotator based on nematic liquid crystal photonic crystal fiber. *J. Lightw. Technol.* IEEE **28**(5), 806–815 (2010)
- Hameed, M.F.O., *et al.*: Modal properties of an index guiding nematic liquid crystal based photonic crystal fiber. *J. Lightw. Technol.* IEEE **27**(21), 4754–4762 (2009a)
- Hameed, M.F.O., Obayya, S.S.A., Wiltshire, R.J.: Multiplexer–demultiplexer based on nematic liquid crystal photonic crystal fiber coupler. *Opt. Quantum Electron.* Springer **41**(4), 315–326 (2009b)
- Hameed, M.F.O., Obayya, S.S.A., El-Mikati, H.A.: Passive polarization converters based on photonic crystal fiber with L-shaped core region. *J. Lightw. Technol.* IEEE **30**(3), 283–289 (2011)
- Hassani, A. and Skorobogatiy, M.: Design of the microstructured optical fiber-based surface plasmon resonance sensors with enhanced microfluidics. *Opt. Express.* **14**(24), 11616–11621 (2006)

- Heinrich, S., et al.: Comparison of ZrN and TiN formed by plasma based ion implantation & deposition. *Surf. Coat. Technol.* Elsevier **202**(11), 2310–2313 (2008)
- Hsu, J.-M., Yao, C.-W., Chen, J.-Z.: Wavelength-tunable dispersion compensating photonic crystal fibers suitable for conventional/coarse wavelength division multiplexing systems. *J. Lightw. Technol.* IEEE **33**(11), 2240–2245 (2015)
- Jabin, M.A., et al.: Surface plasmon resonance based titanium coated biosensor for cancer cell detection. *IEEE Photonics J.* IEEE **11**(4), 1–10 (2019)
- Jindal, S., et al.: Nanocavity-coupled photonic crystal waveguide as highly sensitive platform for cancer detection. *IEEE Sens. J.* IEEE **16**(10), 3705–3710 (2016)
- Kaur, V., Singh, S.: Design of D-Shaped PCF-SPR sensor with dual coating of ITO and ZnO conducting metal oxide. *Optik.* Elsevier **220**, 165135 (2020)
- Klantsataya, E., et al.: Surface plasmon scattering in exposed core optical fiber for enhanced resolution refractive index sensing. *Sens. MDPI* **15**(10), 25090–25102 (2015)
- Koshiba, M. and Tsuji, Y.: Curvilinear hybrid edge/nodal elements with triangular shape for guided-wave problems. *J. Light. Technol.* **18**(5), 737–743 (2000)
- Koshiba, M. and Saitoh, K.: Finite-element analysis of birefringence and dispersion properties in actual and idealized holey-fiber structures. *Appl. Opt.* **42**(31), 6267–6275 (2003)
- Li, W., et al.: ‘An experimental study of pH optical sensor using a section of no-core fiber. *Sens. Actuators A Phys.* Elsevier **199**, 260–264 (2013)
- Liu, S., Jin, L., Jin, W., Wang, D., Liao, C. and Wang, Y.: Structural long period gratings made by drilling micro-holes in photonic crystal fibers with a femtosecond infrared laser. *Opt. Express.* **18**(6), 5496–5503 (2010)
- Liu, L., et al.: V-shaped micro-structure optical fiber surface plasmon resonance sensor for the simultaneous measurement of the refractive index and temperature. *Opt. Lett. Opt. Soc. Am.* **44**(20), 5093–5096 (2019)
- Luan, N., et al.: Surface plasmon resonance sensor based on D-shaped microstructured optical fiber with hollow core. *Opt. Express. Opt. Soc. Am.* **23**(7), 8576–8582 (2015)
- Luo, B., et al.: Novel glucose sensor based on enzyme-immobilized 81 tilted fiber grating. *Opt. Express. Opt. Soc. Am.* **22**(25), 30571–30578 (2014)
- Luo, Y., et al.: ‘Novel optical fiber refractive sensor fabricated with an alcohol-filled photonic crystal fiber based on a Mach-Zehnder interferometer. *Opt. Fiber Technol.* Elsevier **48**, 278–282 (2019)
- Magdi, S., Swillam, M.A.: ‘Investigating several ZrN plasmonic nanostructures and their effect on the absorption of organic solar cells. *J. Phys. D Appl. Phys. IOP Publ.* **50**(38), 385501 (2017)
- Maier, S.A., Atwater, H.A.: ‘Plasmonics: Localization and guiding of electromagnetic energy in metal/dielectric structures. *J Appl. Phys. Am. Ins. Phys.* **98**(1), 10 (2005)
- Malek, C., et al.: Employing the defective photonic crystal composed of nanocomposite superconducting material in detection of cancerous brain tumors biosensor: computational study. *Crystals.* MDPI **12**(4), 540 (2022)
- Migita, S., Morita, Y., Matsukawa, T., Masahara, M., Ota, H.: Experimental demonstration of ultrashort-channel (3 nm) junctionless FETs utilizing atomically sharp V-grooves on SOI. *IEEE Trans Nanotechnol.* **13**(2), 208–215 (2014)
- Mollah, M.A., et al.: Twin core photonic crystal fiber refractive index sensor for early detection of blood cancer. *Sens. Bio-Sens. Res.* Elsevier **29**, 100344 (2020)
- Monfared, Y. E., Kurylyk, B. L. and Dasog, M.: Highly sensitive plasmonic fiber-optic sensors using Group IV transition metal nitrides: a numerical Investigation. *Plasmonics.* Springer, pp. 1–10. (2022)
- Naik, G.V., Shalaev, V.M., Boltasseva, A.: Alternative plasmonic materials: beyond gold and silver. *Adv. Mater.* Wiley Online Library **25**(24), 3264–3294 (2013)
- Nallusamy, N., Raja, R.V.J., Raj, G.J.: Highly sensitive nonlinear temperature sensor based on modulation instability technique in liquid infiltrated photonic crystal fiber. *IEEE Sens. J.* IEEE **17**(12), 3720–3727 (2017)
- Nayak, C.: Numerical study of temperature and pressure effect on one dimensional random photonic crystal used as biosensors in the detection of breast cancer cells. *Phys. Scripta.* IOP Publ. **98**(2), 25503 (2023)
- Obayya, S.S.A., et al.: Full vectorial finite-element-based imaginary distance beam propagation solution of complex modes in optical waveguides. *J. Lightw. Technol.* IEEE **20**(6), 1054 (2002)
- Omri, M., et al.: Highly sensitive photonic sensor based on V-shaped channel mediated gold nanowire. *IEEE Sens. J.* IEEE **20**(15), 8505–8511 (2020)
- Osório, J.H., et al.: Photonic-crystal fiber-based pressure sensor for dual environment monitoring. *Appl. Opt. Opt. Soc. Am.* **53**(17), 3668–3672 (2014)

- Patnaik, A., Senthilnathan, K., Jha, R.: Graphene-based conducting metal oxide coated D-shaped optical fiber SPR sensor. *IEEE Photonics Technol. Lett. IEEE* **27**(23), 2437–2440 (2015)
- Raja, G.T., Varshney, S.K.: Extremely large mode-area bent hybrid leakage channel fibers for lasing applications. *IEEE J. Sel. Top. Quantum Electron. IEEE* **20**(5), 251–259 (2014)
- Rajeswari, D., Revathi, A.A.: Highly sensitive SPR-based PCF bio sensor for plasma cell detection in human blood for the detection of early stage cancer. *Optik. Elsevier* **258**, 168897 (2022)
- Ramanujam, N.R., et al.: Enhanced sensitivity of cancer cell using one dimensional nano composite material coated photonic crystal. *Microsyst. Technol. Springer* **25**(1), 189–196 (2019)
- Rifat, A. A. et al.: Development of photonic crystal fiber-based gas/chemical sensors. In: *Computational photonic sensors*. Springer, pp. 287–317. (2019)
- Sandu, C.S., Sanjinés, R., Medjani, F.: Control of morphology (ZrN crystallite size and SiNx layer thickness) in Zr–Si–N nanocomposite thin films. *Surf. Coat. Technol. Elsevier* **202**(11), 2278–2281 (2008)
- Sani, M.H., Ghanbari, A., Saghaei, H.: ‘High-sensitivity biosensor for simultaneous detection of cancer and diabetes using photonic crystal microstructure. *Opt. Quantum Electron. Springer* **54**, 1–14 (2022)
- Sharan, P. et al.: Design and modelling of photonic sensor for cancer cell detection. In: *2014 International Conference on the IMPact of E-Technology on US (IMPETUS)*. IEEE, pp. 20–24. (2014)
- Sharma, M., Borogohain, N., Konar, S.: Index guiding photonic crystal fibers with large birefringence and walk-off. *J. Lightw. Technol. IEEE* **31**(21), 3339–3344 (2013)
- Shekar, N. C. et al.: Detection of melanoma cancer cell by designing a spr based biosensor. In: *Journal of Physics: Conference Series*. IOP Publishing, p. 12011. (2019)
- Singh, S. and Prajapati, Y. K.: Novel bottom-side polished PCF-based plasmonic biosensor for early detection of hazardous cancerous cells. *IEEE Transactions on NanoBioscience. IEEE*. (2023)
- Soylemez, S., et al.: ‘Electrochemical and optical properties of a conducting polymer and its use in a novel biosensor for the detection of cholesterol. *Sens. Actuators B: Chem Elsevier* **212**, 425–433 (2015)
- Sun, D., et al.: ‘In-situ DNA hybridization detection with a reflective microfiber grating biosensor. *Biosens. Bioelectron Elsevier* **61**, 541–546 (2014)
- Tsai, C. and Huang, S.: Water distribution in cancer and normal cells. Accessed. (2012)
- Verma, P., Kumar, A. and Jindal, P.: Machine learning approach for SPR based photonic crystal fiber sensor for breast cancer cells detection. In: *2022 IEEE 7th Forum on Research and Technologies for Society and Industry Innovation (RTSI)*. IEEE, pp. 7–12. (2022)
- Vigneswaran, D., et al.: Salinity sensor using photonic crystal fiber. *Sens. Actuators A Phys. Elsevier* **269**, 22–28 (2018)
- Villatoro, J., et al.: ‘Temperature-insensitive photonic crystal fiber interferometer for absolute strain sensing. *Appl. Phys. Lett. Am. Ins. Phys.* **91**(9), 91109 (2007)
- Walter, J.-G., et al.: SPR biosensor based on polymer multi-mode optical waveguide and nanoparticle signal enhancement. *Sens. Multidiscip. Digit. Publ. Ins.* **20**(10), 2889 (2020)
- Wang, A., et al.: Side-hole fiber sensor based on surface plasmon resonance. *Opt. Lett. Opt. Publ. Group* **34**(24), 3890–3892 (2009)
- Wang, G., et al.: Highly sensitive D-shaped photonic crystal fiber biological sensors based on surface plasmon resonance. *Opt. Quantum Electron. Springer* **48**(1), 1–9 (2016)
- Wang, J., et al.: Surface plasmon resonance sensor based on coupling effects of dual photonic crystal fibers for low refractive indexes detection. *Res. Phys. Elsevier* **18**, 103240 (2020)
- Wójcik, J., et al.: V type high birefringent PCF fiber for hydrostatic pressure sensing. *Photonics Lett. Poland* **2**(1), 10–12 (2010)
- Wong, W.C., et al.: ‘Photonic crystal fiber surface plasmon resonance biosensor based on protein G immobilization. *IEEE J. Sel. Top. Quantum Electron. IEEE* **19**(3), 4602107 (2013)
- Yaroslavsky, A.N., et al.: High-contrast mapping of basal cell carcinomas. *Opt. Lett. Opt. Soc. Am.* **37**(4), 644–646 (2012)
- Yasli, A.: Cancer detection with surface plasmon resonance-based photonic crystal fiber biosensor. *Plasmon. Springer* **16**, 1605–1612 (2021)
- Yasli, A.: Photonic crystal fiber-based surface plasmon biosensor for breast cancer detection. In: *Proceedings of the 11th International Conference on Robotics, Vision, Signal Processing and Power Applications: Enhancing Research and Innovation through the Fourth Industrial Revolution*. Springer, pp. 709–714. (2022)
- Younis, B.M., et al.: Highly wavelength-selective asymmetric dual-core liquid photonic crystal fiber polarization splitter. *JOSA B. Opt. Soc. Am.* **35**(5), 1020–1029 (2018)
- Yu, X., et al.: Plasmonic enhanced fluorescence spectroscopy using side-polished microstructured optical fiber. *Sens. Actuators B Chem. Elsevier* **160**(1), 196–201 (2011)
- Zhang, S., et al.: Structural and corrosion resistance properties of sputtered zirconium nitride thin films as electrode material for supercapacitor. *J. Alloys Compd. Elsevier* **900**, 163506 (2022)

Zhao, Y., Wu, D., Lv, R.-Q.: Magnetic field sensor based on photonic crystal fiber taper coated with ferrofluid. *IEEE Photonics Technol. Lett. IEEE* **27**(1), 26–29 (2014)

Publisher's Note Springer Nature remains neutral with regard to jurisdictional claims in published maps and institutional affiliations.

Authors and Affiliations

M. Abdelghaffar^{1,3,4} · **Yusuf Gamal**^{2,4} · **Reda A. El-Khoribi**¹ · **Wafaa Soliman**³ · **Y. Badr**³ · **Mohamed Farhat O. Hameed**^{4,5,6} · **S. S. A. Obayya**^{4,7}

M. Abdelghaffar
Mai_makawy2000@yahoo.com

Yusuf Gamal
yusuf.gamal@gmail.com

Reda A. El-Khoribi
r.abdelwahab@fci-cu.du.eg

Wafaa Soliman
wafaamas@niles.edu.eg

Y. Badr
ybadr@niles.edu.eg

¹ Faculty of Computers and Artificial Intelligence, Cairo University, Giza, Egypt

² Engineering Application of Laser Department, National Institute of Laser Enhanced Science (NILES), Cairo University, Giza, Egypt

³ Laser Sciences and Interactions Department, National Institute of Laser Enhanced Science (NILES), Cairo University, Giza, Egypt

⁴ Center for Photonics and Smart Materials, Zewail City of Science, Technology and Innovation, October Gardens, 6th of October City, Giza 12578, Egypt

⁵ Nanotechnology and Nanoelectronics Engineering Program, Zewail City of Science, Technology and Innovation, October Gardens, 6th of October City, Giza 12588, Egypt

⁶ Department of Mathematics and Engineering Physics, Faculty of Engineering, University of Mansoura, Mansoura 35516, Egypt

⁷ Department of Electronics and Communication Engineering, Faculty of Engineering, University of Mansoura, Mansoura 35516, Egypt